Check for updates

Solar RRL

www.solar-rrl.com

Charge Carrier Lifetime Determination in Graded Absorber Solar Cells Using Time-Resolved Photoluminescence Simulations and Measurements

Alexandra M. Bothwell, Carey L. Reich, Adam H. Danielson, Arthur Onno, Zachary C. Holman, Walajabad S. Sampath, and Darius Kuciauskas**

Thin-film photovoltaic device efficiencies are limited by carrier recombination, thus understanding recombination mechanisms is critical for performance improvements. Bulk minority carrier lifetime (τ_{bulk}) is a critical parameter for solar cells but is difficult to determine in P–N junction devices, especially for high doping. As doping $\geq 10^{16}$ cm^{-3} is required for efficient drift-charge-carrier-collection devices, a method for τ_{bulk} determination in doped P–N junction devices is necessary. This work utilizes time-resolved photoluminescence (TRPL) simulations to quantify bulk and interface recombination properties in highly doped, graded absorber CdSeTe structures. The two methods developed here for τ_{bulk} determination include utilization of an instantaneous lifetime representation to guide TRPL fitting and direct comparison between measured and simulated decays. Simulations verified that both methods are valid for state-of-the-art device architectures which include graded bandgap absorbers, graded doping, and graded lifetimes. Shifts in the dominant recombination mechanism are identified for sufficiently long τ_{bulk}, where front and back interface quality plays a more prominent role. Evaluation of surface recombination velocities and conduction band offset illustrate electro-optical advantages of a positive conduction band offset and highlight the necessity of improved interfaces as bulk quality in photovoltaic devices improves.

1. Introduction

Cadmium telluride (CdTe)-based solar cell technology has demonstrated high efficiency, manufacturing growth, and precipitous cost reduction in the last decade.[1,2] Efficiency records of 22.1% for solar cells and 19.1% for modules originated from short-circuit current density (J_{SC}) and fill factor (FF) increases to 99% and 88% of their Shockley–Queisser (SQ) limits, respectively.[2–4] Only ≈79% of the SQ open-circuit voltage (V_{OC}) has been realized, which is attributed to charge carrier recombination.[2–4] Therefore, recombination source identification and mitigation is a primary research focus. This is also the case for all solar cell technologies because defect density reduction in large-area semiconductor structures fabricated by fast growth processes is difficult.

Time-resolved photoluminescence (TRPL) measurements are typically utilized to characterize recombination in direct bandgap material structures and semiconductor solar cells such as CdTe. Electro-optical (EO) properties such as bulk Shockley–Read–Hall (SRH) recombination lifetime (τ_{bulk}), front and back surface recombination velocities (S_{front} and S_{back}), and electron and hole mobilities (μ_e and μ_h), all of which significantly impact solar cell efficiencies,[5–8] can be determined from TRPL decay analysis.[9–13]

Historically, analysis of biexponential TRPL decays included exponential fitting to the initial part of the decay (often called "τ_1") and the tail part of the decay ("τ_2" or "τ_{tail}"). These two regions and their corresponding lifetimes have been used to describe the physical processes of charge separation and minority carrier recombination, respectively.[11] The use of τ_{tail} as an approximation for τ_{bulk} is valid for structures with no P–N junction or space-charge field, such as double heterostructures,[14–16] or when applied voltage partially screens the field.[17] However, in structures with a space charge field and/or increased absorber doping, determination of τ_{bulk} becomes less straightforward: τ_{tail} may over or underestimate τ_{bulk} due to interface recombination, radiative recombination, charge storage, and somewhat subjective fit regions.[17–19] For example, Moseley et al. demonstrated

A. M. Bothwell, D. Kuciauskas
National Renewable Energy Laboratory
Golden, CO 80401, USA
E-mail: a.bothwell3@gmail.com; Darius.Kuciauskas@nrel.gov

C. L. Reich, A. H. Danielson, W. S. Sampath
Department of Mechanical Engineering
Colorado State University
Fort Collins, CO 80523, USA

A. Onno, Z. C. Holman
School of Electrical, Computer and Energy Engineering
Arizona State University
Tempe, AZ 85287, USA

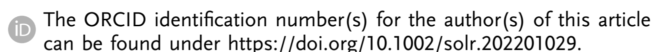
The ORCID identification number(s) for the author(s) of this article can be found under https://doi.org/10.1002/solr.202201029.

© 2023 The Authors. Solar RRL published by Wiley-VCH GmbH. This is an open access article under the terms of the Creative Commons Attribution-NonCommercial-NoDerivs License, which permits use and distribution in any medium, provided the original work is properly cited, the use is non-commercial and no modifications or adaptations are made.

DOI: 10.1002/solr.202201029

2367198x, 2023, 9, Downloaded from https://onlinelibrary.wiley.com/doi/10.1002/solr.202201029 by National Renewable Energy Lab, Wiley Online Library on [08/05/2023]. See the Terms and Conditions (https://onlinelibrary.wiley.com/terms-and-conditions) on Wiley Online Library for rules of use; OA articles are governed by the applicable Creative Commons License

that τ_{tail} correctly approximates τ_{bulk} for SnO_2/CdSeTe/CdTe devices (representative of First Solar's device structures) when absorber acceptor concentration $N_A = 1 \times 10^{14}\,cm^{-3}$ and S_{front}, $S_{back} < 100\,cm\,s^{-1}$.[18] However, charge storage, drift, and radiative recombination effects constrain such determination when $N_A = 1 \times 10^{16}\,cm^{-3}$.[18]

The decline of accurate τ_{bulk} determination for higher doping levels is a significant limitation because doping $N_A \geq 10^{14}\,cm^{-3}$ is needed in photovoltaic devices where minority charge carrier collection is aided by the junction field. Arsenic-doped CdTe devices have reached doping levels of 10^{15}–$10^{16}\,cm^{-3}$,[20–22] $Cu(In,Ga)Se_2$ (CIGS) solar cell doping levels are typically 10^{15}–$10^{16}\,cm^{-3}$ due to intrinsic defects,[23–27] and doping in perovskite solar cells can exceed $10^{16}\,cm^{-3}$.[28] Therefore, bulk recombination lifetime determination in doped absorbers is relevant for multiple PV technologies.

We present a simulation-based approach to understand bulk properties and quantify τ_{bulk} in P–N junction devices, with focus on group V-doped graded cadmium selenium telluride (CdSeTe/CdTe) with $N_A = 1 \times 10^{15}\,cm^{-3}$. Recently, such devices demonstrated high external radiative efficiency (ERE $> 10^{-3}$).[29] CdSeTe/CdTe solar cells have complex absorber composition, with intentionally graded (depth-dependent) absorber bandgap (E_g), lifetime, and radiative efficiency. Thus, we consider the most complex state-of-the-art thin film solar cells. We demonstrate the utility of an instantaneous lifetime representation to provide consistent TRPL fit regions and a route to τ_{bulk} determination. A direct-comparison approach between TRPL measurement and simulation is also implemented for τ_{bulk} determination. We demonstrate that graded $N_A = 1 \times 10^{14}$–$1 \times 10^{15}\,cm^{-3}$ and graded τ_{bulk} have perceptible effects on TRPL decays but neither inhibits the τ_{bulk} analysis methodology developed here. Effects of interfaces are also analyzed, and variation of S_{front} and S_{back} allows for the determination of front or back interface recombination contributions. Finally, the impacts of various EO parameters are illustrated more generally to guide interpretation of TRPL data.

2. Results and Discussion

Carrier dynamics encompass radiative and nonradiative, or Shockley–Read–Hall (SRH), recombination where SRH recombination can be described by bulk, front, and back interface recombination rates

$$\frac{1}{\tau_{TRPL}} = \frac{1}{\tau_{SRH}} + \frac{1}{\tau_{rad}} = \frac{1}{\tau_{bulk}} + \frac{1}{\tau_{front}} + \frac{1}{\tau_{back}} + \frac{1}{\tau_{rad}} \quad (1)$$

τ_{front} corresponds to the minority carrier lifetime associated with recombination at the front (MgZnO/CdSeTe) interface, τ_{back} to the minority carrier lifetime associated with recombination at the back (CdTe/Te) interface, and τ_{rad} is radiative lifetime. Auger recombination is not considered in this work because it is an insignificant recombination mechanism in the direct bandgap CdSeTe/CdTe material. We vary τ_{bulk}, τ_{front}, and τ_{back} to identify recombination limiting mechanisms and compare these simulated results with experimental data.

2.1. Bulk Lifetime Analysis

To investigate bulk recombination, $\tau_{bulk} = 10$, 50, 100, 200, 400, 600, and 1000 ns were used as simulation inputs with $N_A = 1 \times 10^{15}\,cm^{-3}$ and all other input parameters listed in **Table 1**. Interface recombination velocities ($S_{front} = 100\,cm\,s^{-1}$, $S_{back} = 1 \times 10^4\,cm\,s^{-1}$) correspond to values for passivated CdSeTe/CdTe absorbers.[12,30] **Figure 1**a compares simulated TRPL decays for $\tau_{bulk} = 10$, 100, and 1000 ns at excitation fluences 1×10^{11} and 1×10^{12} photons cm^{-2} $pulse^{-1}$. The normalized PL intensity range, 10^{-4}–1, is comparable with the experimentally accessible range in low injection measurements. Figure 1b provides the corresponding instantaneous lifetime, τ_i, profiles, where τ_i is based on the time-derivative of the PL intensity, I_{PL}

$$\tau_i = -\frac{I_{PL}}{\left(\frac{dI_{PL}(t)}{dt}\right)} \quad (2)$$

Instantaneous lifetimes in Figure 1b are analyzed for the PL intensity range in Figure 1a, and therefore do not extend to 2000 ns in all cases. The logarithmic time axis is used to emphasize key aspects of the instantaneous lifetime data. For example, a constant τ_i time range, which originates from unchanging carrier concentration, is visible. In particular, for the case of high bulk recombination ($\tau_{bulk} = 10$ ns) the constant τ_i ($t \approx 2$–30 ns) is approximately equal to τ_{bulk}. This is in good agreement with the widely used TRPL tail-fit approach. For $\tau_{bulk} = 100$ ns, the constant τ_i region extends to later times, and τ_i is slightly less than τ_{bulk} in this range. Instantaneous lifetimes exceed bulk lifetimes at $t > 200$ ns, which has been attributed to charge

Table 1. Simulation parameter inputs for a typical device.

	Parameter	Value
Transparent conducting oxide (TCO)	Thickness	500 nm
	E_g	3.6 eV
	N_D^+	$1 \times 10^{18}\,cm^{-3}$
Buffer (MgZnO)	Thickness	100 nm
	E_g	3.5 eV
	N_D^+	$1 \times 10^{14}\,cm^{-3}$
Absorber (graded CdSeTe)	Thickness	3.0 μm
	Max Se composition [C_0]	0.30
	Carrier concentration, [N_A]	1×10^{14}–$1 \times 10^{15}\,cm^{-3}$
	Absorption coefficient, [α_0]	$1 \times 10^5\,cm^{-1}\,eV^{-0.5}$
	Electron mobility, [μ_e]	$320\,cm^2\,V^{-1}\,s^{-1}$
	Hole mobility, [μ_h]	$40\,cm^2\,V^{-1}\,s^{-1}$
	Rad. recomb. coeff., [B_{rad}]	$2 \times 10^{-10}\,cm^3\,s^{-1}$
Front interface	Conduction band offset	+0.2 eV
	S_{front}	$100\,cm\,s^{-1}$
Back interface	S_{back}	$1 \times 10^4\,cm\,s^{-1}$
	Back hole barrier	0.0 V
Characterization conditions	Laser wavelength	640 nm
	Laser beam diameter	60 μm
	Laser rep. rate	1.1 MHz

© 2023 The Authors. Solar RRL published by Wiley-VCH GmbH

2367198x, 2023, 9, Downloaded from https://onlinelibrary.wiley.com/doi/10.1002/solr.202201029 by National Renewable Energy Lab, Wiley Online Library on [08/05/2023]. See the Terms and Conditions (https://onlinelibrary.wiley.com/terms-and-conditions) on Wiley Online Library for rules of use; OA articles are governed by the applicable Creative Commons License

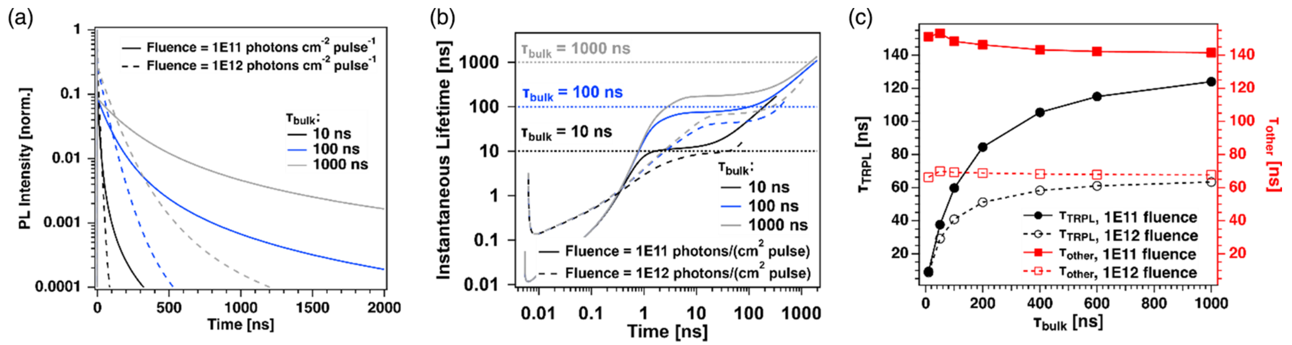

Figure 1. a) Simulated TRPL decays show slower decay with increasing bulk lifetime. Parameters used in simulation are summarized in Table 1, with $N_A = 1 \times 10^{15}$ cm^{-3}. b) Instantaneous lifetime profiles show a constant instantaneous lifetime region which increases in value with greater bulk lifetime. Dotted lines correspond to τ_{bulk} simulation input values. c) "Other" lifetime, which describes the lifetime differential between τ_{bulk} and τ_{TRPL} (fit in the constant τ_i region), is approximately constant as a function of bulk lifetime.

storage.[18,19] For the longest bulk lifetimes ($\tau_{bulk} = 1000$ ns, as reported in passivated structures[31–33]), instantaneous lifetime profiles have similar constant regions, but τ_i does not reach τ_{bulk} value until very late times. This emphasizes that the typical determination of τ_{bulk} by a fit to the tail of a TRPL decay can have a high degree of uncertainty, especially for devices with well-passivated interfaces.

As an alternative to TRPL tail fits, the flat τ_i region can be utilized for τ_{bulk} determination. A single exponential fit to the TRPL decay in the time range where τ_i is constant yields τ_{TRPL}, which is shown as a function of τ_{bulk} on the left axis of Figure 1c. The asymptotic relationship indicates that τ_{TRPL} underestimates τ_{bulk} at long bulk lifetimes which is discussed further in Section 2.3. A re-representation of Equation (1) designates an "other lifetime," τ_{other}, which is comprised of τ_{front}, τ_{back}, and τ_{rad}

$$\frac{1}{\tau_{TRPL}} = \frac{1}{\tau_{bulk}} + \frac{1}{\tau_{front}} + \frac{1}{\tau_{back}} + \frac{1}{\tau_{rad}} = \frac{1}{\tau_{bulk}} + \frac{1}{\tau_{other}} \quad (3)$$

The difference between $\tau_{bulk}{}^{-1}$ and $\tau_{TRPL}{}^{-1}$ enables calculation of τ_{other} which, as shown on the right axis of Figure 1c, is approximately constant as a function of τ_{bulk}. Given the dependence of τ_{TRPL} on fluence, τ_{other} is also dependent on fluence such that $\tau_{other} \approx 143$ ns for 1×10^{11} photons cm^{-2} pulse^{-1} and ≈ 68 ns for 1×10^{12} photons cm^{-2} pulse^{-1}.

To determine τ_{bulk} from a measured TRPL decay, this process can be reversed: rate $\tau_{other}{}^{-1}$, determined from the above-outlined simulation with values specific to the device structure and measurement conditions, is added to $\tau_{TRPL}{}^{-1}$ to arrive at τ_{bulk} according to Equation (3).

This approach has a few limitations. First, devices should have $\tau_{bulk} > 100$ ns because τ_{other} is not constant at lower values. Second, it is also limited to TRPL measured at somewhat low fluence, $<1 \times 10^{13}$ photons cm^{-2} pulse^{-1}. At higher fluences, presented in the supplementary section, the flat τ_i region disappears because the photogenerated carrier concentration is high enough that the carrier concentration profiles change across all time intervals. Finally, this approach requires EO parameter and device composition knowledge. For example, if the back interface is changed, the simulation process must be repeated with a new S_{back} value. The effects of altered parameters on instantaneous lifetime are provided in the Supporting Information.

A second method for τ_{bulk} determination is through comparison between simulated and measured TRPL. **Figure 2**a shows TRPL data of As-doped structures (described in the Experimental Section) with a standard Te/C/Ni back contact (gray) and a passivating Al_2O_3/a-Si/ITO/Ag back contact (blue). Because the difference in these samples is the back contact structure, it can be reasonably assumed that the different TRPL tail lifetimes (102 ns for standard back contact and 166 ns for passivated back contact) can be attributed to variation in S_{back}. Thus, simulations were executed with τ_{bulk} varied and equal between samples, and S_{back} varied and unequal between samples.

Figure 2a show good agreement between measured and simulated decays for $\tau_{bulk,max} = 450$ ns (where $\tau_{bulk,max}$ corresponds to the maximum bulk lifetime in the graded absorber as shown in Figure 8b) and $S_{back} = 5 \times 10^3$ and 800 cm s^{-1} for the standard and passivated back contacts, respectively. The bulk lifetime is longer than the tail fit results which emphasizes the uncertainty in TRPL fitting. This is expected based on Figure 1b,c results discussed above: for long τ_{bulk} with fluence $= 1 \times 10^{12}$ photons cm^{-2} pulse^{-1}, a fit to TRPL decay data at $t > \approx 200$ ns will underestimate actual τ_{bulk}.

Figure 2b shows the instantaneous lifetime profiles from the simulated decays. This highlights how changes in S_{back} materialize in the TRPL decay: the most prominent difference is exhibited in the flat τ_i region. This is discussed in greater detail in Section 2.3.

2.2. Effects of Grading: Bulk Lifetime and Absorber Doping

Alloyed CdSeTe and group V doping are grading sources in CdTe device structures. This grading is used in all high-efficiency CdTe solar cells (as well as CIGS solar cells), and it is therefore critical to understand its impact. Multiple properties are depth-dependent (graded), and we consider three important categories. Graded bandgap, E_g, is included in all simulations and was implemented in Section 2.1. Here, we additionally consider effects due to grading of minority carrier lifetime (graded

© 2023 The Authors. Solar RRL published by Wiley-VCH GmbH

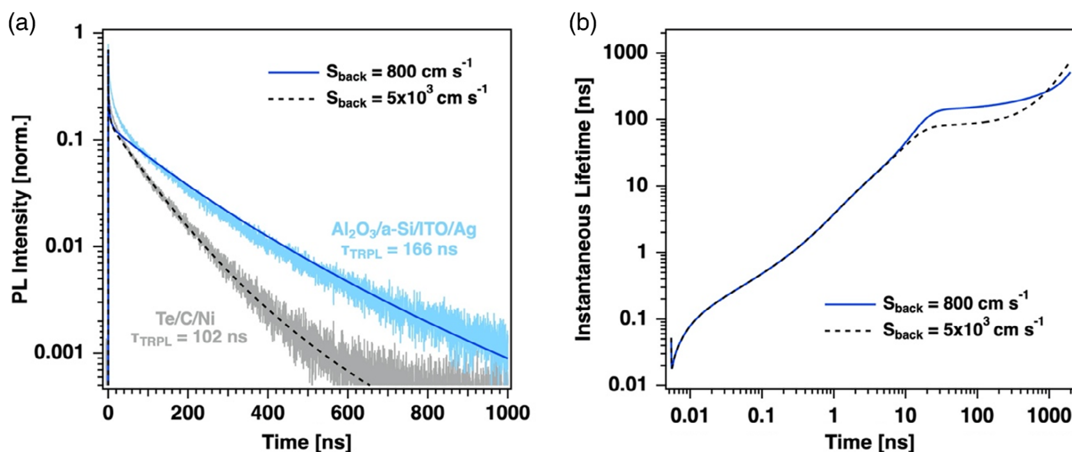

Figure 2. a) Measured TRPL decays of As-doped graded CdSeTe/CdTe structures with standard Te/C/Ni back contact (gray) and a passivating Al_2O_3/a-Si/ITO/Ag back contact (blue) compared to simulated decays suggest $\tau_{bulk,max} = 450$ ns and $S_{back} = 5 \times 10^3$ and 800 cm s^{-1} for the standard and passivated back contacts, respectively. b) Instantaneous lifetimes from the simulated decays highlight the greatest difference occurs in the flat τ_i region.

τ_{bulk}) and absorber dopant density (graded N_A). Because these properties are harder to measure, analysis is based on simulations.

The opposite τ_{bulk} and N_A grading profiles (Figure 8b) originate from chemical composition and the method used to dope the absorber. Greater τ_{bulk} near the front junction is due to the higher Se content. This was confirmed in experiments on nongraded absorbers with varying Se composition[33] and through cathodoluminescence (CL) measurements which consistently indicate higher radiative efficiency in regions with more Se.[34] In contrast to Se composition, N_A is higher at the back of the device due to the doping process which is enacted by As diffusion from the back of the structure. This approach mitigates effects of As accumulation near the front interface where As accumulation can lead to increased interface recombination.[22,35–37] The analytical models describing graded τ_{bulk} and N_A profiles are approximations sufficient for this analysis.[21,22]

Figure 3a,c compares simulated TRPL decays and instantaneous lifetime profiles with and without τ_{bulk} grading, given a fixed acceptor carrier concentration $N_A = 1 \times 10^{15}$ cm^{-3}. For short- and mid-range τ_{bulk}, 10 and 100 ns respectively, τ_{bulk} grading alters τ_i in value but not time range of the flat τ_i region. At longer τ_{bulk}, 1000 ns, the grading has a much smaller effect on the TRPL decay: only small reductions in τ_i in the flat τ_i region are apparent. More specifically, there is a 20% relative decrease in τ_i for $\tau_{bulk} = 10$ ns, a 16% relative decrease for $\tau_{bulk} = 100$ ns, and a 4% relative decrease for $\tau_{bulk} = 1000$ ns. Overall, the effect of τ_{bulk} grading in this device structure is small, especially with long bulk lifetimes. This indicates that a 50% τ_{bulk} grading profile should have only a small impact on TRPL interpretation.

Figure 3b,d compares TRPL decays and instantaneous lifetime profiles with and without N_A grading. Carrier concentration grading has a more notable effect than τ_{bulk} grading: the initial and flat τ_i time regions are both impacted. The early-time TRPL behavior, which is influenced in part by minority carrier drift, changes because the electric field is modified by varied carrier concentration. The flat τ_i region narrows and τ_i decreases for lower carrier concentration. For the graded case $N_A = 1 \times 10^{14}$–1×10^{15} cm^{-3}, the flat τ_i range is closer to $N_A = 1 \times 10^{15}$ cm^{-3} than $N_A = 1 \times 10^{14}$ cm^{-3}, indicating the dominance of the more highly doped region. This implies that with a transition from a traditional Cu-doped device ($N_A = 1 \times 10^{14}$ cm^{-3}) to a graded, As-doped device ($N_A = 1 \times 10^{14}$–1×10^{15} cm^{-3}) one should expect a wider, higher value τ_i region in addition to the slower TRPL decays observed with As doping.[22,32,35]

Grading results indicate that the utilization of the flat τ_i region for TRPL fitting as described in the previous section is still applicable for absorbers with graded τ_{bulk} and N_A. The flat τ_i time range is slightly narrowed by N_A grading, and the value changes slightly due to both τ_{bulk} and N_A grading, but it is still appropriate for τ_{TRPL} extraction and τ_{other} calculation.

2.3. Interface Recombination

2.3.1. Interface and Bulk Rate Relationships

Interface properties were investigated through varied front and back interface recombination velocity (S_{front} and S_{back}) simulation inputs. This analysis underscores how recombination-limiting mechanisms depend on the interplay of τ_{bulk} and S_{front} and S_{back}. We first consider cases when $S_{front} = S_{back}$ and advance to variation of these values independently.

Figure 4a compares simulations for the representative ("typical") device structure discussed in the previous sections to the ideal interfaces case ($S_{front} = S_{back} = 1$ cm s^{-1}; such ideal interfaces have been realized in single crystal CdTe[38]), with $\tau_{bulk} = 10$, 100, and 1000 ns. The difference between ideal versus typical interfaces becomes increasingly significant for longer bulk lifetimes as the dominant recombination mechanism shifts from bulk recombination to interface recombination. The τ_i profiles in Figure 4b reveal that the recombination velocity modifications change TRPL decay in the flat τ_i time range. In the case of short $\tau_{bulk} = 10$ ns, the flat τ_i values agree well with τ_{bulk} because

© 2023 The Authors. Solar RRL published by Wiley-VCH GmbH
2367198x, 2023, 9, Downloaded from https://onlinelibrary.wiley.com/doi/10.1002/solr.202201029 by National Renewable Energy Lab, Wiley Online Library on [08/05/2023]. See the Terms and Conditions (https://onlinelibrary.wiley.com/terms-and-conditions) on Wiley Online Library for rules of use; OA articles are governed by the applicable Creative Commons License

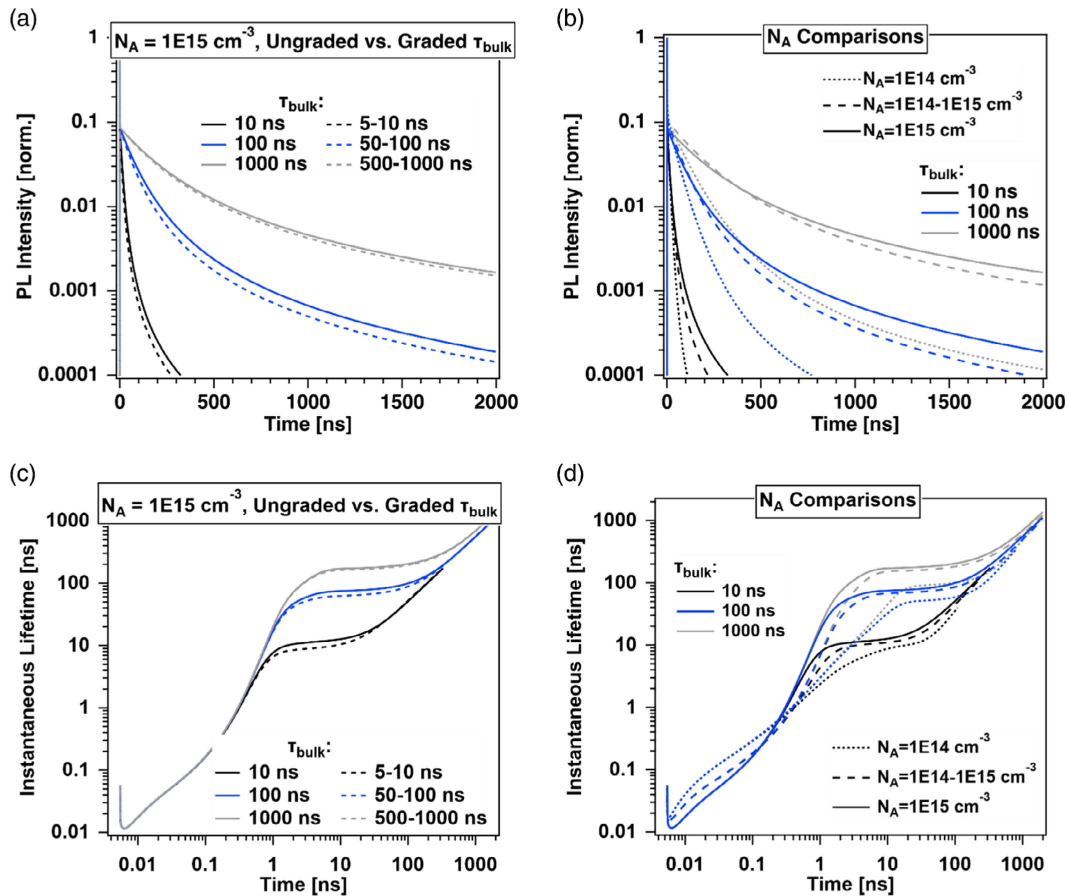

Figure 3. a) Simulated TRPL decays and c) instantaneous lifetime profiles show that bulk lifetime grading changes the value of the flat instantaneous lifetime region. Solid lines correspond to ungraded bulk lifetimes and dashed lifetimes correspond to graded bulk lifetimes. b) TRPL decays and d) instantaneous lifetime profiles show that N_A grading changes the value and time range of the flat instantaneous lifetime region.

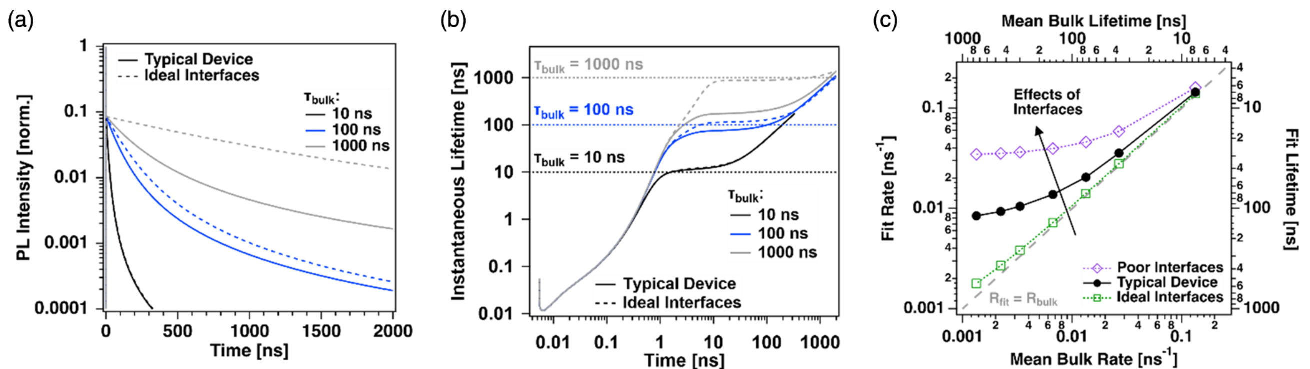

Figure 4. a) Simulated TRPL decays and b) instantaneous lifetime profiles for typical and ideal device interfaces with $N_A = 1 \times 10^{15}$ cm. c) Mean rates and lifetimes extracted from the flat τ_i region when graded bulk lifetime is varied. Interface effects are seen most prominently at short bulk rates (long bulk lifetimes). The following parameters are used in simulations: typical device: $S_{front} = 100$ cm s^{-1}, $S_{back} = 1 \times 10^4$ cm s^{-1}. Ideal interfaces: $S_{front} = S_{back} = 1$ cm s^{-1}. Poor interfaces: $S_{front} = 1 \times 10^4$ cm s^{-1}, $S_{back} = 1 \times 10^5$ cm s^{-1}.

it is the dominant recombination mechanism, and the effect of improved interfaces is negligible. As τ_{bulk} increases, interface recombination plays a more dominant role; long τ_{bulk} is only well matched by τ_i if interface recombination velocities are low. In agreement with earlier sections, the flat τ_i region is the critical TRPL decay time range in which recombination-limiting mechanisms can be explored.

The impact of interface recombination is summarized in Figure 4c which shows TRPL fit rate R_{TRPL} (fit lifetime τ_{TRPL}) versus mean bulk rate R_{bulk} (graded lifetime τ_{bulk}) for simulated

© 2023 The Authors. Solar RRL published by Wiley-VCH GmbH

2367198x, 2023, 9, Downloaded from https://onlinelibrary.wiley.com/doi/10.1002/solr.202201029 by National Renewable Energy Lab, Wiley Online Library on [08/05/2023]. See the Terms and Conditions (https://onlinelibrary.wiley.com/terms-and-conditions) on Wiley Online Library for rules of use; OA articles are governed by the applicable Creative Commons License

$\tau_{bulk,max} = 10$–1000 ns in the case of ideal, typical, and poor interfaces. Lifetime τ_{TRPL} was determined by a single exponential TRPL fit in the flat τ_i time range and fit rate was calculated as τ_{TRPL}^{-1}. The gray, dashed line represents the case without interface or radiative recombination ($R_{TRPL} = R_{bulk}$, $\tau_{TRPL} = \tau_{bulk}$). The R_{TRPL} versus R_{bulk} representation emphasizes the increasing impact of interfaces for longer τ_{bulk}: data essentially overlap at high bulk rates (short τ_{bulk}) where bulk recombination is dominant and deviate from $R_{TRPL} = R_{bulk}$ as τ_{bulk} improves. Increasingly poor interfaces are apparent at low bulk rates (long τ_{bulk}) where interface recombination becomes the dominant recombination mechanism.

Figure 4c suggests that in a device with poor interfaces ($S_{front} = 1 \times 10^4$ cm s^{-1}, $S_{back} = 1 \times 10^5$ cm s^{-1}) bulk defect density reduction (improvements to τ_{bulk}) will not increase τ_{TRPL} above ≈30 ns. In typical devices ($S_{front} = 100$ cm s^{-1}, $S_{back} = 1 \times 10^4$ cm s^{-1}), τ_{TRPL} is limited to ≈100 ns. Therefore, as CdSeTe/CdTe bulk lifetimes continue to increase, there is an accompanied need for improved interfaces.

The impact of defects at front and back interfaces was investigated by analysis of TRPL sensitivity to independently varied S_{front} and S_{back} inputs. As excitation (and solar irradiation) occurs through the front interface and carriers are generated close to the front contact, S_{front} impact on overall recombination might be expected to be higher. Alternatively, the electric field near the front interface (due to the P–N junction and absorber grading) might reduce the impact of S_{front}. Simulation results in **Figure 5** enable an understanding of these contributions. Figure 5a,b present a case where S_{front} and S_{back} differ by 10^4 cm s^{-1} and Figure 5c,d a case where S_{front} and S_{back} differ by 100 cm s^{-1}. We consider short bulk lifetimes (Figure 5a,c) and long bulk lifetimes (Figure 5b,d). The ideal case, $S_{front} = S_{back} = 1$ cm s^{-1}, is given by the dashed lines for reference.

In all cases, S_{front} has a greater impact on lifetime than S_{back}, demonstrated by the higher τ_i values for a minimized S_{front}. However, this impact is somewhat small, especially for the typical device structure that has been discussed (SRVs = 100 and 1×10^4 cm s^{-1}). These results hold regardless of bulk lifetime (compare Figure 5a,c–b,d). This suggests that regardless of absorber quality, reduction of S_{front} would be somewhat more favorable for improved carrier lifetime than S_{back} reduction. But data indicate that without at least one ideal interface, the differences are small.

Next, to quantify interface recombination rate, R_{int} is calculated by (compare with Equation (1))

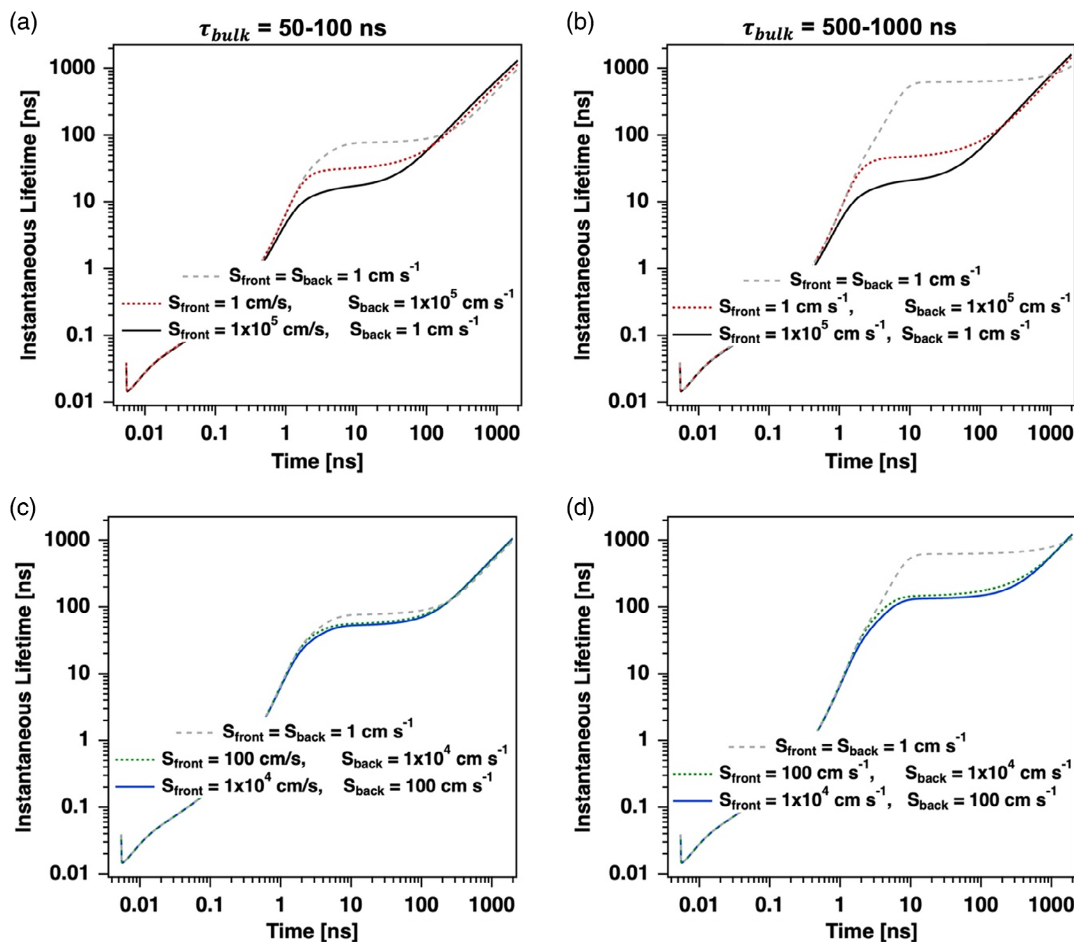

Figure 5. Instantaneous lifetime profiles with interchanged S_{front} and S_{back} for a,c) $\tau_{bulk} = 50$–100 and b,d) 500–1000 ns. Dashed gray lines correspond to ideal interfaces $S_{front} = S_{back} = 1$ cm s^{-1}. Results indicate that S_{front} impacts TRPL more when the SRV differential is large.

© 2023 The Authors. Solar RRL published by Wiley-VCH GmbH

2367198x, 2023, 9, Downloaded from https://onlinelibrary.wiley.com/doi/10.1002/solr.202201029 by National Renewable Energy Lab, Wiley Online Library on [08/05/2023]. See the Terms and Conditions (https://onlinelibrary.wiley.com/terms-and-conditions) on Wiley Online Library for rules of use; OA articles are governed by the applicable Creative Commons License

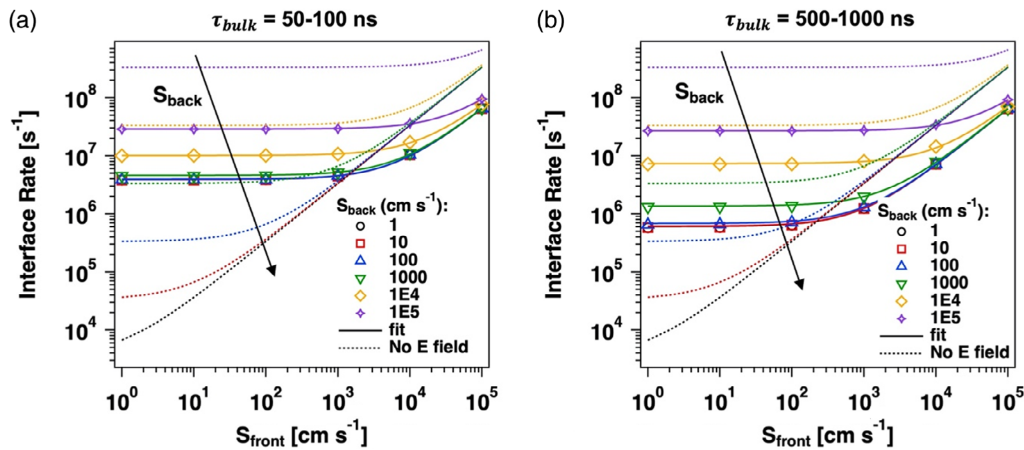

Figure 6. Interface rates as a function of S_{front} and S_{back} for graded τ_{bulk} = 50–100 ns (a) and 500–1000 ns (b). Symbols are device simulation results and solid lines are corresponding fits to Equation (5) with independent fit parameters d for both interfaces. Dotted lines plot a field-free sample: Equation (5) where d is sample thickness.

$$R_{int} = R_{TRPL} - R_{bulk} - R_{rad} \tag{4}$$

where $R_{rad} = N_A B_{rad}$ under a low injection condition like that investigated here. R_{int} versus S_{front} with discrete S_{back} values are given in **Figure 6**a,b for graded $\tau_{bulk} = 50$–100 and 500–1000 ns, respectively. Simulation results for devices, determined by Equation (4), are given by symbols. For samples without electric field[14]

$$R_{int} = S_{front}/d + S_{back}/d \tag{5}$$

where d is absorber thickness and recombination velocities derive from the interface defect density, N_{int} ($S \approx v_{th}\sigma N_{int}$, where v_{th} is thermal velocity and σ is capture cross section). The dotted lines in Figure 6 show R_{int} calculated from Equation (5) for samples without an electric field; in most cases agreement with device simulations is poor.

The solid lines in Figure 6 apply the model of Equation (5) to the simulation results but adjust parameter d in the fit, independently for each interface. Employment of d as a floating parameter for fits creates a more realistic device description where carriers do not equally see each interface. Because fitted d values differ from the sample thickness, the fits indicate how the impact of front and/or back interface recombination differs in structures without an electric field versus devices. Comparison of solid lines (device) and dotted lines (absorber without electric field) shows that interface rates can be both higher and lower in devices, depending on τ_{bulk}, S_{front}, and S_{back}.

2.3.2. Interface and Conduction Band Offset Relationships

The front-side conduction band offset (CBO) between the n-type buffer and p-type absorber (MgZnO and CdSeTe, respectively, in the structures presented here) significantly impacts carrier recombination and open-circuit voltage (V_{OC}), where V_{OC} is maximized with CBO = +0.2 eV for MgZnO/CdSeTe device structures.[39,40] Here, we present the impact that CBO has on interface recombination.

Figure 7 compares interface recombination rates (determined by Equation (4)) for CBO = 0.0 eV (Figure 7a,c) and +0.2 eV (Figure 7b,d) with variation in S_{front} and S_{back}. For CBO = +0.2 eV, the symmetric contours indicate that S_{front} and S_{back} contribute nearly equally to interface recombination. In contrast, for CBO = 0.0 eV interface recombination is affected primarily by S_{front}. This indicates that with a spike-like, +0.2 eV CBO, improvement to the front or back interface will equally reduce interface recombination but with a flat band, 0.0-eV CBO, interface recombination is limited by S_{front}. These conclusions hold for short and long bulk lifetimes, exemplified by the unchanged contour symmetries in Figure 7a,c and b,d, with graded $\tau_{bulk} = 50$–100 and 500–1000 ns.

The different scales between Figure 7a,c and b,d highlight that CBO also impacts the range of achievable interface rates. This range is significantly lower and narrower for CBO = +0.2 eV than 0.0 eV. This indicates that CBO = +0.2 eV is superior for reduced interface recombination, in agreement with V_{OC} and efficiency simulation and experimental results in the literature.[39,40]

Finally, the CBO has little impact on late decay times, which is discussed in greater detail in the supplementary material section. Therefore, to investigate CBO with TRPL, early decay times should be utilized. Results in the supplementary material show that variation of CBO has a smaller effect than properties analyzed in Section 2.1–2.3.1.

3. Conclusion

Minority carrier lifetime is a central parameter in PV materials. For Si PV, lifetimes are measured for wafers rather than devices. This is not viable for thin films where absorber properties change in device fabrication. Therefore, to determine carrier lifetimes in thin film solar cells, simulations of lifetime measurements such as TRPL are used. In this article, a simulation-based lifetime analysis methodology was developed which categorizes dominant carrier recombination mechanisms and enhances bulk

© 2023 The Authors. Solar RRL published by Wiley-VCH GmbH

2367198x, 2023, 9, Downloaded from https://onlinelibrary.wiley.com/doi/10.1002/solr.202201029 by National Renewable Energy Lab, Wiley Online Library on [08/05/2023]. See the Terms and Conditions (https://onlinelibrary.wiley.com/terms-and-conditions) on Wiley Online Library for rules of use; OA articles are governed by the applicable Creative Commons License

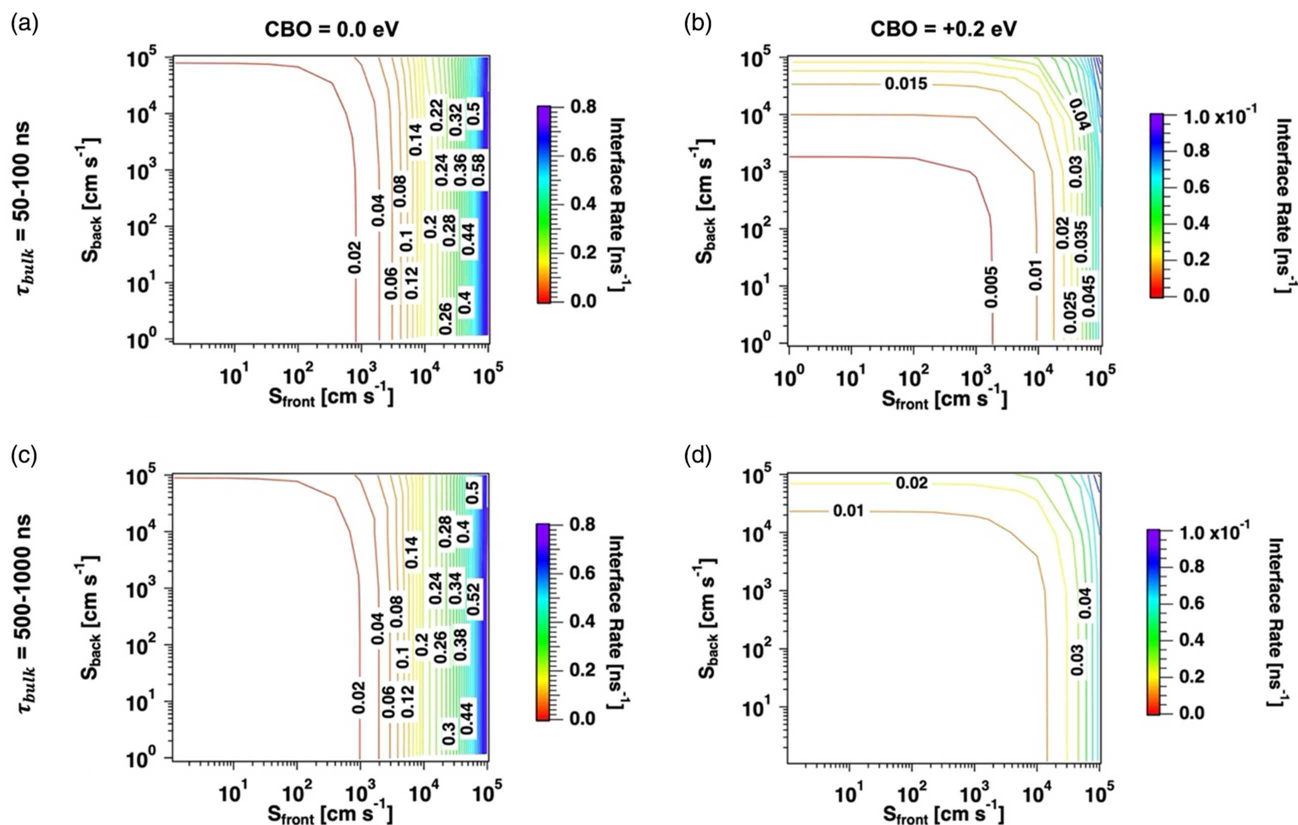

Figure 7. Interface rates as a function of S_{front} and S_{back} for τ_{bulk} = 50–100 ns (a,b) and 500–1000 ns (c,d) for CBOs = 0 eV and +0.2 eV, respectively.

carrier lifetime determination for graded absorber CdSeTe solar cells doped at 10^{15} cm^{-3}.

Two TRPL simulation methods were developed to reduce the ambiguity of bulk lifetime determination in group V-doped CdSeTe devices with a P–N junction. First, the flat instantaneous lifetime region was utilized to establish a well-defined TRPL fit range compared to the often-indefinite tail fit region in traditional TRPL fitting processes. This flat τ_i region was used to calculate τ_{bulk}. Second, comparisons between simulations and measured TRPL data provided more explicit bulk lifetime quantification as well as information about additional electro-optical properties.

Graded lifetimes and acceptor carrier concentrations—associated with long-lifetime graded CdSeTe absorbers and high, group V doping at the back of devices—impacted TRPL decay shapes but did not nullify the τ_{bulk} determination methods described above. τ_{bulk} grading had a non-negligible impact at short bulk lifetimes and less impact at longer bulk lifetimes. Carrier concentration grading demonstrated a change in early-time TRPL behavior due to the electric field modification by carrier concentration gradients, as well as at later times where τ_i decreased for lower carrier concentration.

The flat τ_i region also highlighted recombination-limiting mechanisms. The difference in τ_i between ideal and typical interface cases increased significantly for longer τ_{bulk}, dictated by the shift in dominant recombination mechanism from bulk to interface recombination. This highlights the necessity of improved interfaces as CdSeTe bulk quality improves. Independent impacts of front and back interface recombination velocities revealed that S_{front} has a somewhat greater impact on fit lifetime than S_{back}, although this impact is fairly small, especially for the typical CdSeTe device which was primarily discussed. Comparison of flat-band, 0.0 eV and spike-like, +0.2 eV front-side CBOs demonstrated the advantages of a positive CBO. It reduces interface recombination, in agreement with V_{OC} and efficiency simulation and experimental results in the literature.[39,40] These results can be utilized to direct research focus between bulk and interface defect density reduction for a more targeted approach to photovoltaic efficiency increases.

4. Experimental Section

COMSOL Simulation: TRPL decays were simulated using a COMSOL application,[41] in which the time-dependent electron and hole continuity equations and Poisson's equation are solved after pulsed laser excitation to generate recombination rate components. Carrier generation is from the front, or glass-side of a superstrate-configured device, and as described by Moseley et al., many additional parameters can be varied as simulation inputs.[18] The simulation application is publicly available.[41]

Simulation inputs were established based on the As-doped CdSeTe devices fabricated at Colorado State University which were measured for experimental comparison. The device structure is given in **Figure 8**a. Absorber composition grading, which is consistent throughout this work, is given by $y(x) = C_0\text{erf}(x/L)$ with exponential-like decreasing Se

© 2023 The Authors. Solar RRL published by Wiley-VCH GmbH

2367198x, 2023, 9, Downloaded from https://onlinelibrary.wiley.com/doi/10.1002/solr.202201029 by National Renewable Energy Lab, Wiley Online Library on [08/05/2023]. See the Terms and Conditions (https://onlinelibrary.wiley.com/terms-and-conditions) on Wiley Online Library for rules of use; OA articles are governed by the applicable Creative Commons License

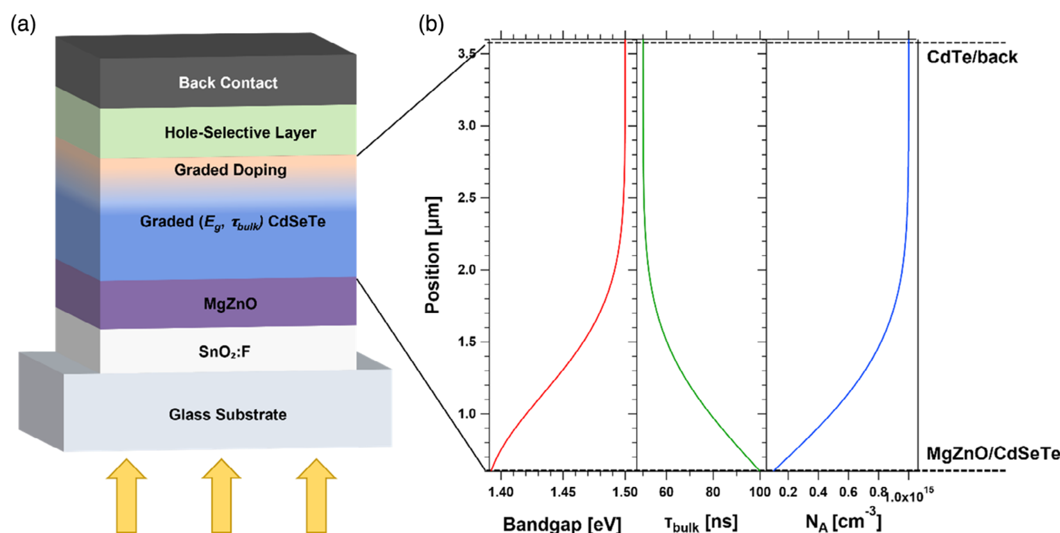

Figure 8. a) Graded CdSeTe/CdTe absorber structure (not to scale). b) Bandgap, bulk lifetime, and acceptor concentration grading in the absorber are assumed to derive from chemical composition and follow similar grading profiles.

composition from the front to back interface. y is the fraction of anion sites occupied by Se, C_0 is maximum Se composition, x is absorber depth, and L is a length-scaling constant. Composition grading dictates the absorber bandgap, $E_g(y) = 1.5(1-y) + 1.7y - 0.8y(1-y)$.[18] Here, $C_0 = 0.30$ and $L = 1$ µm such that E_g varies from 1.39 eV at the front MgZnO/CdSeTe interface to 1.50 eV at the back interface as shown in Figure 8b.[34,42] Figure 8a,b also highlights the additional graded parameters, τ_{bulk} and N_A, investigated in this work. Additional input parameters are given in Table 1 with values held fixed unless otherwise specified.[6,12,22,39]

Structure Fabrication and Characterization: Structures were fabricated on a SnO_2:F/100 nm MgZnO substrate. The first device architecture was 0.5 µm CdSeTe:As/2.6 µm CdTe/200 nm CdSeTe:As/Te/C/Ni, referred to as the standard back contact, and the second was 0.5 µm CdSeTe/3.0 µm CdTe/200 nm CdSeTe:As/Al_2O_3/a-Si/ITO/Ag, referred to as the passivated back contact. Structures were not delineated into individual devices. The *n*-type MgZnO buffer layer was RF sputter-deposited on SnO_2:F-coated glass (Pilkington Tec10), followed by close-space sublimation-deposited CdSeTe and CdTe and $CdCl_2$ passivation treatment. Devices were As-doped through a cosublimation process under Cd overpressure using predoped $CdSe_{0.4}Te_{0.6}$ material. Acceptor concentration in finished devices was $N_A \approx 1 \times 10^{15}$ cm^{-3} for both structures, measured by capacitance–voltage. Standard back contact devices were finished with 30 nm of evaporated Te and spray-coated carbon and nickel paints. Passivated devices were finished with a 2 nm magnetron sputtered Al_2O_3 layer followed by an 8 nm p-type boron-doped hydrogenated amorphous silicon (a-Si:H(p)) layer deposited by plasma-enhanced chemical vapor deposition, and finally, a 70 nm ITO/200 nm Ag back electrode was deposited by reactive sputtering. Additional fabrication details can be found in the literature.[12,29]

TRPL was measured using excitation at 640 nm with fluence $= 1.0 \times 10^{12}$ photons cm^{-2} $pulse^{-1}$, incident on the front MgZnO/CdSeTe side of the structure. Excitation wavelength was controlled by an optical parametric amplifier (OPA) and 0.3 ps pulses at a 1.1 MHz repetition rate were used. Time-correlated single photon counting was implemented for TRPL decay detection.[43]

Supporting Information

Supporting Information is available from the Wiley Online Library or from the author.

Acknowledgements

This work was authored in part by the National Renewable Energy Laboratory, operated by Alliance for Sustainable Energy, LLC, for the U.S. Department of Energy (DOE) under Contract No. DE-AC36-08GO28308. Funding provided by U.S. Department of Energy Office of Energy Efficiency and Renewable Energy Solar Energy Technologies Office. The views expressed in the article do not necessarily represent the views of the DOE or the U.S. Government. This article has been contributed to by US Government contractors and their work is in the public domain in the USA. The information, data, or work presented herein was funded in part by the U.S. Department of Energy, Office of Energy Efficiency and Renewable Energy, under award number DE-EE0008552.

Conflict of Interest

The authors declare no conflict of interest.

Data Availability Statement

The data that support the findings of this study are available from the corresponding author upon reasonable request.

Keywords

carrier lifetime, doping, interfaces, solar cells, time-resolved photoluminescence

Received: November 15, 2022
Revised: January 13, 2023
Published online: February 28, 2023

[1] S. Philipps, Photovoltaics Report, Fraunhofer Institute for Solar Energy Systems ISE Press and Public Relations, Freiburg, Germany **2022**.
[2] M. A. Scarpulla, B. McCandless, A. B. Phillips, Y. Yan, M. J. Heben, C. Wolden, G. Xiong, W. K. Metzger, D. Mao, D. Krasikov, I. Sankin,

© 2023 The Authors. Solar RRL published by Wiley-VCH GmbH

2367198x, 2023, 9, Downloaded from https://onlinelibrary.wiley.com/doi/10.1002/solr.202201029 by National Renewable Energy Lab, Wiley Online Library on [08/05/2023]. See the Terms and Conditions (https://onlinelibrary.wiley.com/terms-and-conditions) on Wiley Online Library for rules of use; OA articles are governed by the applicable Creative Commons License

2367198x, 2023, 9, Downloaded from https://onlinelibrary.wiley.com/doi/10.1002/solr.202201029 by National Renewable Energy Lab, Wiley Online Library on [08/05/2023]. See the Terms and Conditions (https://onlinelibrary.wiley.com/terms-and-conditions) on Wiley Online Library for rules of use; OA articles are governed by the applicable Creative Commons License

S. Grover, A. Munshi, W. Sampath, J. R. Sites, A. Bothwell, D. Albin, A. Romeo, M. Nardone, R. Klie, J. M. Walls, T. Fiducia, A. Abbas, *Sol. Energy Mater. Sol. Cells*, **2023**, accepted.

[3] M. Green, E. Dunlop, J. Hohl-Ebinger, M. Yoshita, N. Kopidakis, X. Hao, *Prog. Photovoltaics: Res. Appl.* **2021**, *29*, 3.

[4] R. M. Geisthardt, M. Topič, J. R. Sites, *IEEE J. Photovolt.* **2015**, *5*, 1217.

[5] G. K. Liyanage, A. B. Phillips, F. K. Alfadhili, R. J. Ellingson, M. J. Heben, *ACS Appl. Energy Mater.* **2019**, *2*, 5419.

[6] R. Pandey, T. Shimpi, A. Munshi, J. R. Sites, *IEEE J. Photovolt.* **2020**, *10*, 1918.

[7] J. N. Duenow, W. K. Metzger, *J. Appl. Phys.* **2019**, *125*, 053101.

[8] A. Kanevce, M. O. Reese, T. Barnes, S. Jensen, W. Metzger, *J. Appl. Phys.* **2017**, *121*, 214506.

[9] D. Kuciauskas, in *Advanced Characterization of Thin Film Solar Cells* (Eds: M. Al-Jassim, N. Haegel), IET Energy Engineering Series, Vol. *166*, London, UK **2020**.

[10] M. Maiberg, C. Spindler, E. Jarzembowski, R. Scheer, *Thin Solid Films* **2015**, *582*, 379.

[11] A. Kanevce, D. Levi, D. Kuciauskas, *Prog. Photovolt. Res. Appl.* **2014**, *22*, 1138.

[12] A. Danielson, D. Kuciauskas, C. Reich, S. Li, A. Onno, W. Weigand, A. Kindvall, A. Munshi, Z. Holman, W. Sampath, *47th IEEE Photovoltaic Specialists Conf. (PVSC)*, IEEE, Piscataway, NJ **2020**, pp. 1811–1812.

[13] A. Kanevce, D. Kuciauskas, T. A. Gessert, D. H. Levi, D. S. Albin, *38th IEEE Photovoltaic Specialists Conf.*, IEEE, Piscataway, NJ **2012**, pp. 000848–000853.

[14] K. N. Zaunbrecher, D. Kuciauskas, C. H. Swartz, P. Dippo, M. Edirisooriya, O. S. Ogedengbe, S. Sohal, B. L. Hancock, E. G. LeBlanc, P. A. Jayathilaka, *Appl. Phys. Lett.* **2016**, *109*, 091904.

[15] R. K. Ahrenkiel, *Semicond. Semimetals* **1993**, *39*.

[16] E. Perl, D. Kuciauskas, J. Simon, D. Friedman, M. Steiner, *J. Appl. Phys.* **2017**, *122*, 233102.

[17] P. M. Jundt, D. Kuciauskas, J. R. Sites, *IEEE J. Photovolt.* **2021**, *12*, 501.

[18] J. Moseley, D. Krasikov, C. Lee, D. Kuciauskas, *J. Appl. Phys.* **2021**, *130*, 163105.

[19] M. Maiberg, T. Hölscher, S. Zahedi-Azad, R. Scheer, *J. Appl. Phys.* **2015**, *118*, 105701.

[20] W. K. Metzger, S. Grover, D. Lu, E. Colegrove, J. Moseley, C. Perkins, X. Li, R. Mallick, W. Zhang, R. Malik, *Nat. Energy* **2019**, *4*, 837.

[21] E. Colegrove, B. Good, A. Abbas, H. Moutinho, S. Johnston, C.-S. Jiang, P. O'Keefe, J. M. Walls, D. S. Albin, M. O. Reese, *Sol. Energy Mater. Sol. Cells* **2022**, *246*, 111886.

[22] A. Danielson, C. Reich, R. Pandey, A. Munshi, A. Onno, W. Weigand, D. Kuciauskas, S. Li, A. Bothwell, J. Guo, M. Murugeson, J. S. McCloy, Z. C. Holman, W. Sampath, *Sol. Energy Mater. Sol. Cells* **2023**, *251*, 112110.

[23] N. Mufti, T. Amrillah, A. Taufiq, M. Diantoro, H. Nur, *Sol. Energy* **2020**, *207*, 1146.

[24] M. Asaduzzaman, M. Hasan, A. N. Bahar, *SpringerPlus* **2016**, *5*, 1.

[25] S. Shirakata, *Phys. Status Solidi C* **2017**, *14*, 1600170.

[26] Y. Sun, S. Lin, W. Li, S. Cheng, Y. Zhang, Y. Liu, W. Liu, *Engineering* **2017**, *3*, 452.

[27] A. J. Ferguson, R. Farshchi, P. K. Paul, P. Dippo, J. Bailey, D. Poplavskyy, A. Khanam, F. Tuomisto, A. R. Arehart, D. Kuciauskas, *J. Appl. Phys.* **2020**, *127*, 215702.

[28] J. Tong, Q. Jiang, A. J. Ferguson, A. F. Palmstrom, X. Wang, J. Hao, S. P. Dunfield, A. E. Louks, S. P. Harvey, C. Li, *Nat. Energy* **2022**, *7*, 642.

[29] A. Onno, C. Reich, S. Li, A. Danielson, W. Weigand, A. Bothwell, S. Grover, J. Bailey, G. Xiong, D. Kuciauskas, W. S. Sampath, Z. C. Holman, *Nat. Energy* **2022**, *7*, 400.

[30] D. Kuciauskas, J. M. Kephart, J. Moseley, W. K. Metzger, W. S. Sampath, P. Dippo, *Appl. Phys. Lett.* **2018**, *112*, 263901.

[31] D. Kuciauskas, D. Albin, J. Moseley, S. Li, P. Ščajev, C. Reich, A. H. Munshi, A. Danielson, W. Sampath, C. Lee, *47th IEEE Photovoltaic Specialists Conf. (PVSC)*, IEEE, Piscataway, NJ **2020**, pp. 0082–0084.

[32] A. H. Munshi, C. L. Reich, A. H. Danielson, R. Pandey, D. Kuciauskas, J. Guo, S. Li, A. Shah, S. Swain, T. M. Shimpi, *47th IEEE Photovoltaic Specialists Conf. (PVSC)*, IEEE, Piscataway, NJ **2020**, pp. 1824–1828.

[33] M. Amarasinghe, D. Albin, D. Kuciauskas, J. Moseley, C. L. Perkins, W. K. Metzger, *Appl. Phys. Lett.* **2021**, *118*, 211102.

[34] T. A. Fiducia, B. G. Mendis, K. Li, C. R. Grovenor, A. H. Munshi, K. Barth, W. S. Sampath, L. D. Wright, A. Abbas, J. W. Bowers, *Nat. Energy* **2019**, *4*, 504.

[35] D. L. McGott, E. Colegrove, J. N. Duenow, C. A. Wolden, M. O. Reese, *ACS Energy Lett.* **2021**, *6*, 4203.

[36] J. Guo, A. Sharma, A. Munshi, C. Reich, A. Danielson, W. Sampath, S. Swain, R. Klie, *Microsc. Microanal.* **2020**, *26*, 1232.

[37] B. Good, E. Colegrove, M. O. Reese, *Sol. Energy Mater. Sol. Cells* **2022**, *246*, 111928.

[38] Y. Zhao, M. Boccard, S. Liu, J. Becker, X.-H. Zhao, C. M. Campbell, E. Suarez, M. B. Lassise, Z. Holman, Y.-H. Zhang, *Nat. Energy* **2016**, *1*, 1.

[39] R. Pandey, A. Munshi, T. Shimpi, A. Shah, A. Bothwell, D. Kuciauskas, J. R. Sites, *Sol. RRL* **2021**, *5*, 2100126.

[40] T. Ablekim, E. Colegrove, W. K. Metzger, *ACS Appl. Energy Mater.* **2018**, *1*, 5135.

[41] Thin-Film Solar Cell Current Voltage and Time-Resolved Photoluminescence Simulation Model. https://www.nrel.gov/pv/solar-cell-jv-trpl-simulation-model.html, (accessed: November **2022**).

[42] A. H. Munshi, J. Kephart, A. Abbas, J. Raguse, J.-N. Beaudry, K. Barth, J. Sites, J. Walls, W. Sampath, *IEEE J. Photovolt.* **2017**, *8*, 310.

[43] D. Kuciauskas, J. N. Duenow, A. Kanevce, J. V. Li, M. R. Young, P. Dippo, D. H. Levi, *38th IEEE Photovoltaic Specialists Conf.*, IEEE, Piscataway, NJ **2012**, pp. 001721–001726.

© 2023 The Authors. Solar RRL published by Wiley-VCH GmbH